

# Selenium isotopes record extensive marine suboxia during the Great Oxidation Event

Michael A. Kipp<sup>a,b,1</sup>, Eva E. Stüeken<sup>a,b,c,d</sup>, Andrey Bekker<sup>c</sup>, and Roger Buick<sup>a,b</sup>

<sup>a</sup>Department of Earth & Space Sciences and Astrobiology Program, University of Washington, Seattle, WA 98195-1310; <sup>b</sup>Virtual Planetary Laboratory, NASA Astrobiology Institute, Seattle, WA 98195-1310; <sup>c</sup>Department of Earth Sciences, University of California, Riverside, CA 92521; and <sup>d</sup>Department of Earth & Environmental Sciences, University of St. Andrews, St. Andrews, KY16 9AL, Scotland, United Kingdom

Edited by Mark H. Thiemens, University of California, San Diego, La Jolla, CA, and approved December 13, 2016 (received for review September 24, 2016)

It has been proposed that an “oxygen overshoot” occurred during the early Paleoproterozoic Great Oxidation Event (GOE) in association with the extreme positive carbon isotopic excursion known as the Lomagundi Event. Moreover, it has also been suggested that environmental oxygen levels then crashed to very low levels during the subsequent extremely negative Shunga–Francevillian carbon isotopic anomaly. These redox fluctuations could have profoundly influenced the course of eukaryotic evolution, as eukaryotes have several metabolic processes that are obligately aerobic. Here we investigate the magnitude of these proposed oxygen perturbations using selenium (Se) geochemistry, which is sensitive to redox transitions across suboxic conditions. We find that  $\delta^{82/78}\text{Se}$  values in offshore shales show a positive excursion from 2.32 Ga until 2.1 Ga (mean  $+1.03 \pm 0.67\%$ ). Selenium abundances and Se/TOC (total organic carbon) ratios similarly show a peak during this interval. Together these data suggest that during the GOE there was pervasive suboxia in near-shore environments, allowing nonquantitative Se reduction to drive the residual Se oxyanions isotopically heavy. This implies  $\text{O}_2$  levels of  $>0.4 \mu\text{M}$  in these settings. Unlike in the late Neoproterozoic and Phanerozoic, when negative  $\delta^{82/78}\text{Se}$  values are observed in offshore environments, only a single formation, evidently the shallowest, shows evidence of negative  $\delta^{82/78}\text{Se}$ . This suggests that there was no upwelling of Se oxyanions from an oxic deep-ocean reservoir, which is consistent with previous estimates that the deep ocean remained anoxic throughout the GOE. The abrupt decline in  $\delta^{82/78}\text{Se}$  and Se/TOC values during the subsequent Shunga–Francevillian anomaly indicates a widespread decrease in surface oxygenation.

Paleoproterozoic | trace metals | oxygen | eukaryote evolution

The accumulation of molecular oxygen in Earth’s atmosphere and ocean fundamentally restructured biogeochemical pathways, and ultimately allowed the evolution of aerobically respiring eukaryotic life. Determining the tempo of the rise of oxygen to modern levels has thus been the focus of decades of research (1, 2). The beginning of the Paleoproterozoic Era (2.5–1.6 Ga) is of particular interest, because it was the first time in Earth’s history when oxygen-rich conditions prevailed in surface environments for a prolonged interval (3).

The first permanent step in the oxygenation of Earth’s surface, the Great Oxidation Event (GOE), was originally identified by the disappearance of redox-sensitive detrital minerals (4, 5) and the appearance of red beds (6) around the Archean–Proterozoic boundary. More recently, the record of mass-independent fractionation of sulfur isotopes (MIF-S) in sedimentary sulfates and sulfides (7) revealed that atmospheric  $\text{O}_2$  increased from negligible amounts to  $>10^{-5}$  times present atmospheric levels (8) between 2.45 and 2.32 Ga, which is now thought to mark the onset of the GOE (9, 10).

Although its name may seem to imply a discrete upward step in the oxidation state of Earth’s surface, a new view is emerging of the GOE as a dynamic interval of rising and then falling  $\text{O}_2$  lasting until  $\sim 2.06$  Ga (3, 11). The occurrence of the largest and longest-lived positive carbon isotope excursion in the geologic record—the Lomagundi Event (LE) (12)—in the later stages of the GOE

between 2.22 and 2.06 Ga, has been cited as evidence of enhanced organic carbon burial that may have allowed high levels of free oxygen to temporarily accumulate at Earth’s surface at this time (13), i.e., an “oxygen overshoot” (3).

Indeed, there is mounting evidence for expansion and contraction of the marine sulfate reservoir across the LE (14–16), which is thought to reflect trends in oxidative sulfide weathering and oxygenation of the ocean as atmospheric oxygen levels rose and fell. Relative iodate abundances in carbonates also document an increase in shallow-water oxidation state near the onset of the GOE, peaking during the LE (17). Additionally, enrichments of molybdenum (Mo) and uranium (U) in organic-rich shales reflect vigorous oxidative weathering of the continents during the GOE (18, 19). Thus, a fairly consistent picture is emerging of an  $\text{O}_2$ -rich world between  $\sim 2.3$  and 2.1 Ga.

However, whereas the above proxies have indicated widespread oxygen availability in the early Paleoproterozoic, we still lack precise constraints on the extent of oxic, suboxic, and anoxic (including euxinic) habitats in the oceans at this time. This is a matter of great evolutionary importance, because the spatial and temporal transience of oxic-to-suboxic environments may have been the dominant throttle on eukaryotic evolution before the late Neoproterozoic (0.8–0.54 Ga) (20). If oxygenated habitats were indeed abundant during the GOE, it could have constituted the first time in Earth’s history that geographically extensive regions of the ocean were conducive to the evolution of complex life.

Accurately probing the redox landscape of the oceans during the GOE requires a suite of proxies that function at different spatial scales. Evidence for large marine sulfate, iodate, Mo, and U reservoirs is suggestive of a global expansion of oxygenated water masses. However, these signals lack the resolution to assess

## Significance

Oxygen is essential for eukaryotic life. The geologic record of early Earth contains abundant evidence of low oxygen levels, and accordingly, a lack of eukaryote fossils. The rise of oxygen to near-modern levels at the end of the Proterozoic Era is thus often cited as the trigger for the evolutionary radiation of complex life forms at this same time. Here we present selenium geochemical data that indicate an expansion of suboxic ( $>0.4 \mu\text{M O}_2$ ) habitats in the shallow oceans between 2.32 and 2.1 Ga—more than one billion years before eukaryotes become abundant in the fossil record. These environments could have harbored the earliest stages of eukaryotic evolution, but may have been too transient for substantial diversification to occur.

Author contributions: M.A.K., E.E.S., A.B., and R.B. designed research; M.A.K. and E.E.S. performed research; M.A.K. and E.E.S. analyzed data; and M.A.K., E.E.S., A.B., and R.B. wrote the paper.

The authors declare no conflict of interest.

This article is a PNAS Direct Submission.

<sup>1</sup>To whom correspondence should be addressed. Email: kipp@uw.edu.

This article contains supporting information online at [www.pnas.org/lookup/suppl/doi:10.1073/pnas.1615867114/-DCSupplemental](http://www.pnas.org/lookup/suppl/doi:10.1073/pnas.1615867114/-DCSupplemental).

basinal redox gradients that could be critical for eukaryote ecology. Conversely, Fe speciation is a well-developed local redox indicator, and has been used to identify euxinia in offshore environments during the GOE (16, 21). But, because this signal records local conditions, with spatially limited data it lacks the ability to distinguish an oxygen-minimum zone in an otherwise globally oxic ocean from a globally anoxic deep ocean.

Selenium (Se) is well-suited for bridging the gaps between the aforementioned proxies, as its relatively short oceanic residence time ( $\sim 10^3$  y) makes Se sensitive to basin-scale redox dynamics. Selenium is predominantly delivered to the oceans via oxidative weathering, making the marine Se reservoir scale with continental oxidative weathering rates. Additionally, Se isotopes can be fractionated by several permil during oxyanion ( $\text{SeO}_4^{2-}$ ,  $\text{SeO}_3^{2-}$ ,  $\text{HSeO}_3^-$ ) reduction to elemental Se and selenide in suboxic environments, such as modern oxygen-minimum zones and suboxic pore waters. In these settings, if Se oxyanions are continuously supplied from oxygenated waters, reduction is nonquantitative and the resulting isotopic values of reduced Se compounds are typically negative (22, 23). Negative Se isotope ratios in sedimentary rocks can therefore be an indication that the sediments were deposited in an environment that was linked to a large oxic reservoir. Selenium isotopes have been used in this way to track the oxygenation of the deep ocean in the late Neoproterozoic, where fractionations down to  $-1.5\text{‰}$  have been recorded in offshore shales that received upwelling Se oxyanions from oxic deep oceans (24). In modern anoxic basins where Se oxyanions are not continuously resupplied, Se is largely consumed by uptake into biomass without net fractionation and the reduction of Se oxyanions is quantitative (25). Isotopic values in these settings are therefore typically heavy, approaching or exceeding the composition of seawater, which is  $\sim +0.3\text{‰}$  today (23).

We measured Se abundance and isotope ratios in organic-rich shales from seven stratigraphic units deposited in offshore environments during and after the GOE. These lithologies capture the offshore Se reservoir, which records basin-scale redox structure. Viewed together, these snapshots of individual basins at different stages of the GOE offer a glimpse of secular changes in the redox structure of the global ocean. Our results thus provide a proxy record that can test the predictions made by other redox-sensitive indicators and help resolve the spatial and temporal distribution of oxic, suboxic, and anoxic marine environments during the GOE. Specifically, these data allow us to test whether the Paleoproterozoic oxygen overshoot was at any time comparable in magnitude to the Neoproterozoic oxygenation event, and to assess the implications for the early evolution of eukaryotic life.

## Materials

We analyzed 75 samples from 7 shale units deposited between 2.2 and 1.85 Ga. These data were compared with 567 published Se measurements from samples with ages spanning 3.25 Ga to the present. Samples corresponding to the early stage of the GOE come from the Rooihooft and Timeball Hill formations of the Pretoria Group (2.32 Ga), which were analyzed by Stüeken et al. (23), and are the oldest open-marine shales deposited without an MIF-5 signature. In addition, we sampled the Wewe Slate ( $\sim 2.2$ – $2.1$  Ga) and Sengoma Argillite Formation ( $\sim 2.2$ – $2.1$  Ga), which were deposited in the middle of the GOE, during the Lomagundi carbon isotope excursion. Samples straddling the end of the GOE and Lomagundi carbon isotope excursion come from the Hautes Chutes Formation of the Labrador Trough ( $\sim 2.1$  Ga), the Francevillian Series of Gabon ( $\sim 2.083$  Ga), the Zaonega Formation of Karelia, Russia ( $\sim 2.11$ – $2.06$  Ga), and the Union Island Group of the Slave craton ( $\sim 2.1$ – $2.0$  Ga). In addition, organic-rich shales of the Menihok Formation from the Labrador Trough (1.85 Ga), postdating the LE, were also analyzed. These samples span the latest stages of the GOE and the 200 My interval after its termination, and include the formations in which the Shunga-Francevillian negative carbon isotope anomaly was originally discovered (11).

## Results

Shales deposited in offshore environments show a broad trend in Se concentrations across the GOE, with abundances increasing

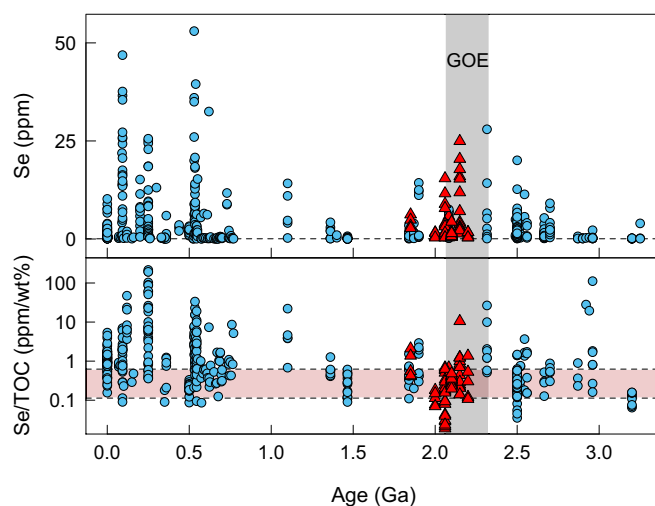


**Fig. 1.** Se abundance and Se/TOC (ppm/wt %) ratios in shales through geologic time (triangles, this study; circles, published data). Dotted lines represent crustal Se abundance (Top) and range of Se/TOC ratios in modern phytoplankton (22) (Bottom).

in the late Archean and subsequently falling through the Paleoproterozoic, with a peak between 2.32 and 2.1 Ga (max. 27.97 ppm; Fig. 1). Mean Se abundance of shales deposited between 2.32 and 2.1 Ga (6.79 ppm) is significantly higher than the mean Se abundance for shales older than 2.45 Ga (2.04 ppm;  $p_{\text{one-tailed}} = 10^{-8}$ ) and with ages between 2.1 and 1.1 Ga (2.02 ppm;  $p_{\text{one-tailed}} = 10^{-8}$ ). Se/TOC (total organic carbon) ratios similarly show a peak (max. 26.84 ppm/wt %) in the early stage of the GOE, but rapidly decline between 2.1 and 2.0 Ga to  $<< 1$  ppm/wt % (Figs. 1 and 2).

$\delta^{82/78}\text{Se}$  values are consistently positive from 2.32 Ga until 2.1 Ga, and higher than in any other time in the geologic record (avg.  $+1.03 \pm 0.67\text{‰}$ ; Figs. 2 and 3). The mean  $\delta^{82/78}\text{Se}$  value for samples older than 2.45 Ga is statistically indistinguishable from that for samples dating between 2.1 and 1.1 Ga ( $p_{\text{two-tailed}} = 0.11$ ), whereas samples with 2.32–2.1 Ga ages have significantly higher  $\delta^{82/78}\text{Se}$  values than both groups ( $p_{\text{one-tailed}} = 10^{-10}$ ,  $10^{-10}$ ). Negative  $\delta^{82/78}\text{Se}$  values do not become prevalent until the late Neoproterozoic (24), and persist throughout the Phanerozoic (23) (Fig. 3).

**Oxidative Weathering and the Marine Se Reservoir.** In light of mounting evidence for elevated atmospheric oxygen levels between 2.32 and 2.06 Ga (3, 15–19), it is unsurprising that shales show an increase in Se abundance at this time (Fig. 1). Whereas Se can also be sourced to the marine environment by volcanism and hydrothermal activity, oxidative weathering is by far the dominant source on the modern Earth ( $\sim 90\%$  of flux to oceans; volcanism  $\sim 10\%$ , hydrothermal input  $<< 1\%$ ; ref. 26). Furthermore, the parallel enrichment of U (19), Mo (18), and Se in samples from the Rooihooft and Lower Timeball Hill formations and the Sengoma Argillite Formation is most parsimoniously explained by enhanced oxidative weathering. Unlike Se, U is exclusively delivered to the oceans via oxidative mobilization, and not by volcanic or hydrothermal inputs. Additionally, Mo is not volatile and thus cannot derive from volcanic sources. Although it is not possible to definitively rule out a volcanic contribution to the sedimentary Se enrichment seen during the GOE, the vast majority of Se was likely delivered by oxidative continental weathering.

The trend in Se abundance does not correspond exactly with the inferred beginning and end of the GOE (Fig. 1). Se concentrations begin to increase in the late Archean ( $\sim 2.7$  Ga), perhaps due to increasing rates of oxidative weathering in locally oxic environments on land (27). In the wake of the GOE, Se abundances remain higher than mid-Archean values until at least 1.9 Ga, and



This leaves partial reduction of Se oxyanions as the most likely process to generate large ( $>1\%$ ) fractionations that can be preserved in sedimentary rocks. In laboratory settings, both biotic and abiotic partial reduction generate isotopic fractionations of several permil, with lighter Se isotopes being preferentially enriched in reduced compounds (33). In bulk samples from natural settings, observed fractionations tend to be smaller (range from  $-2$  to  $+2\%$ ), perhaps because the isotopic signature of reduced Se gets diluted by codeposition of biologically assimilated Se in sediments (34). Still, dissimilatory reduction can alter the Se isotopic composition of residual oxyanions dissolved in seawater, and this has been documented in the Phanerozoic (35), Neoproterozoic (24), and Archean (36). In the 2.5 Ga Mt. McRae Shale, Se isotopes show a positive excursion parallel with a positive excursion in nitrogen isotopes and enrichments in redox-sensitive trace metals that have been interpreted as evidence for a transient pulse of oxygen that occurred before the onset of the GOE (36–38). Stüeken et al. (36) argued that this Se isotope excursion was generated in a redox-stratified water column where Se was partially reduced in shallow-marine, suboxic waters, driving the residual Se reservoir to more positive  $\delta^{82/78}\text{Se}$  values, which were then recorded in offshore shales. The positive  $\delta^{82/78}\text{Se}$  values seen during the GOE seem to indicate a similar scenario, although in this instance persisting in multiple basins on separate continents over a timescale of hundreds of millions of years.

The fact that most sedimentary Se isotope ratios in Archean and mid-Proterozoic shales do not significantly deviate from crustal values (Fig. 3) suggests that either Se influx was generally low or that Se oxyanions in the oceans during these intervals were quantitatively reduced and assimilated (Fig. 4A), allowing sediments to roughly record the isotopic composition of crustal source rocks. The observation of significantly positive  $\delta^{82/78}\text{Se}$  values in all analyzed offshore sediments dating within the GOE thus suggests an extreme isotopic distillation of an expanded marine Se reservoir at this time. To generate such a large isotopic excursion, there were likely extensive near-shore suboxic environments where Se oxyanions were constantly resupplied, allowing substantial nonquantitative reduction to occur in the water column. This would sequester isotopically light Se in near-shore sediments that were not sampled in this study, perhaps with the exception of the Wewe Slate (see below) (Fig. 4B). The residual Se reservoir would thus have been driven isotopically heavy. These heavy values could then have been recorded in the offshore environments sampled in this study either by quantitative or nonquantitative reduction and/or biological assimilation, depending on the extent of suboxia on the outer shelf.

This stands in contrast to the modern ocean, which receives a large flux of Se oxyanions but generates only small isotopic fractionations (Fig. 4C). Suboxic waters are scarce in the fully oxygenated modern oceans ( $<10\%$  of ocean area; ref. 39) and diagenetic Se reduction in sediments seems to produce relatively small fractionations, perhaps because the supply of Se oxyanions is diffusion-limited in pore waters. Thus, the magnitude of the positive  $\delta^{82/78}\text{Se}$  excursion seen in shales deposited during the GOE suggests that suboxia was a widespread and persistent feature along continental margins during this interval.

The lack of negative  $\delta^{82/78}\text{Se}$  values in offshore sediments deposited during the GOE also suggests that—unlike in the late Neoproterozoic and Phanerozoic—there was not any resupply of Se oxyanions from an oxic deep-ocean reservoir. This is consistent with previous work that has suggested the deep ocean remained anoxic throughout the GOE (40). So, whereas the Se data alone remain somewhat ambiguous as to the precise redox state of the sampled offshore depositional environments, they can be used to confidently infer the persistence of widespread near-shore suboxia, and predominantly anoxic conditions in the deep ocean.

An isotopic record of Se in near-shore sediments that preserve the complementary negative  $\delta^{82/78}\text{Se}$  values and were deposited coevally with the shales bearing the positive  $\delta^{82/78}\text{Se}$  excursion

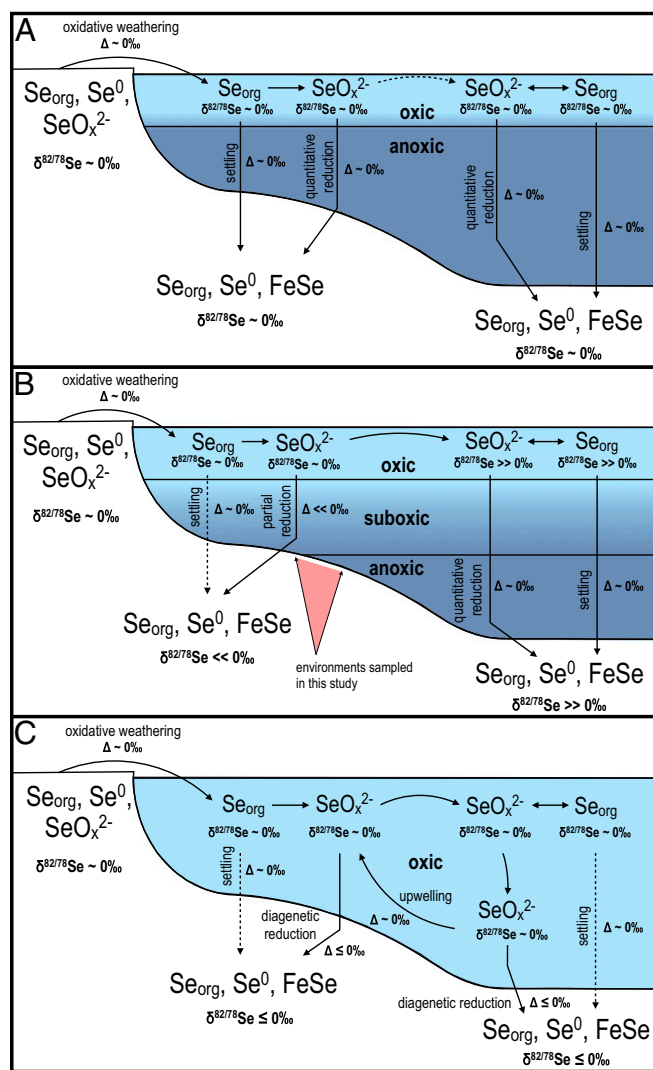


**Fig. 4.** Sketch of the selenium cycle during (A) the late Archean and mid-Proterozoic, (B) the Great Oxidation Event, and (C) the late Neoproterozoic and Phanerozoic. " $\delta^{82/78}\text{Se}$ " refers to the isotope ratio of a designated reservoir; " $\Delta$ " refers to the isotopic fractionation associated with a designated process. Dotted arrows for  $\text{Se}_{\text{org}}$  burial in oxic/suboxic environments signify that this process has minor significance, but in some cases may dilute sedimentary Se isotope signatures (34). See text for further discussion.

would provide a test of this hypothesis. However, given current sensitivity limits for Se isotope analysis, this remains a challenging prospect. Se concentrations in carbonates, sandstones, and low-TOC shales associated with near-shore depositional environments are orders of magnitude less than in offshore organic-rich shales, requiring unfeasibly large sample sizes to obtain accurate measurements. Further methodological refinement may eventually enable analysis of such materials.

Still, there is some evidence for a complementary light Se reservoir in shallow-water environments during the GOE. The Wewe Slate ( $\sim 2.2\text{--}2.1$  Ga) displays by far the largest range of  $\delta^{82/78}\text{Se}$  values of units analyzed in this study ( $-1.34$  to  $+2.25\%$ ; Dataset S1). We suspect that this is because this unit is capturing the seawater Se composition near the environmental gradient for Se reduction. The Wewe Slate is underlain by mature quartz sandstones and stromatolitic dolostones (41) and has relatively low TSe and TOC contents (Fig. 1, SI Appendix), all consistent with a near-shore depositional environment, in contrast to the TSe- and

TOC-rich shales from other units included in this dataset. Because there is no noticeable stratigraphic trend in Se isotopes or abundance through the Weve Slate (*SI Appendix*), it is unlikely that the range of values reflects secular change in the depositional environment. We cannot rule out the possibility that the Weve Slate is capturing transient deep-ocean oxygenation in the midst of the GOE, but the sedimentologic context is consistent with deposition of the Weve Slate in a setting that straddled a chemocline with fluctuating depth, thus sampling both the shallow and deep Se reservoirs.

At the end of the GOE (2.1–2.0 Ga),  $\delta^{82/78}\text{Se}$  values sharply return to crustal values (Fig. 2), consistent with rapid deoxygenation of the ocean (16). The occurrence of some negative  $\delta^{82/78}\text{Se}$  values in the Zaonega and Francevillian formations may result from the weathering of isotopically light Se that was deposited in shallow settings during the GOE, and subsequently uplifted and eroded on tectonic timescales of  $\sim 100$  My. However, we cannot definitively rule out the possibility that these data represent a pulse of oxygenation at the culmination of the GOE (11). In either case, the longer-term trend reveals an ultimate return to widespread anoxia. Even if Se influx to the ocean decayed gradually as Se-rich sediments deposited during the GOE were weathered, a contraction of suboxic water masses and takeover by anoxic and strongly euxinic conditions could have rapidly pushed the system toward quantitative reduction of Se oxyanions, thus ending the Se isotopic excursion seen during the GOE. Contraction of the marine Se reservoir during deoxygenation would further accelerate the loss of isotopic fractionation, because a smaller Se reservoir could be quantitatively reduced more easily.

**How Oxic Were Near-Shore Environments During the GOE?** These data can be used to provide an approximate lower limit on shallow-marine oxygen levels across the GOE. Specifically, when used in conjunction with the iodine record, the Se data point to the presence of conditions that were at least suboxic. In the modern ocean, quantitative reduction of iodate ( $\text{IO}_3^-$ ) to iodide ( $\text{I}^-$ ) has been observed at dissolved  $\text{O}_2$  concentrations less than  $\sim 5 \mu\text{M}$  (42). In the same study, Se oxyanion reduction was nonquantitative at oxygen concentrations down to  $\sim 1 \mu\text{M}$   $\text{O}_2$ . Another investigation of Se speciation in the anoxic Saanich Inlet found that Se oxyanions became depleted to below the detection limit at  $< 0.4 \mu\text{M}$   $\text{O}_2$  (25). Within this framework, the occurrence of positive  $\delta^{82/78}\text{Se}$  values across the GOE implies a conservative lower limit for shallow-water oxygen concentrations of  $> 0.4 \mu\text{M}$   $\text{O}_2$ . In reality, it is likely that  $\text{O}_2$  concentrations were higher in these settings, because reduction of Se oxyanions in near-shore environments was evidently far from being quantitative. High  $\text{I}/(\text{Ca} + \text{Mg})$  ratios in LE-aged carbonates (17) may push the lower limit for surface ocean oxygen up to  $\sim 5 \mu\text{M}$   $\text{O}_2$  for the later stage of the GOE. This would still only be a small fraction of the modern surface ocean oxygen concentration of  $\sim 325 \mu\text{M}$   $\text{O}_2$ , but it could have had important evolutionary implications.

**Implications for Biological Evolution.** Whether or not oxygen availability was the primary control on the evolution of deeply rooted eukaryotes remains a highly contentious issue. Recent evidence for extremely low mid-Proterozoic oxygen levels (43) has hinted that low oxygen indeed inhibited the diversification of multicellular, aerobically respiring organisms until the late Neoproterozoic (see ref. 44 for an alternative view). However, the recognition of oxygen-rich conditions in the early Paleoproterozoic opens up the possibility that there was a relatively long ( $\sim 200$  My) interval that may have been favorable for the evolution of complex life forms long before the fossil record indicates their rise to ecological importance (45, 46).

Convincing fossil evidence of multicellular eukaryotic life is hard to come by in the Proterozoic, but there are numerous reports of

fossils purported to have eukaryotic affinity that span nearly the entire temporal extent of the Proterozoic (47–49). These include centimeter-scale structures in the  $\sim 2.1$  Ga Francevillian Series of Gabon that have been interpreted as populations of multicellular organisms (50). While such reports remain controversial, a better understanding of the redox architecture of the contemporary oceans would greatly aid our interpretation of the possible affinities of these ambiguous fossilized life forms.

The observed lower limit for survival of aerobically respiring benthic animals is  $\sim 0.88 \mu\text{M}$   $\text{O}_2$  (51, 52), and theoretical considerations suggest that the actual limit is even lower (53). For steroid synthesis in unicellular eukaryotes, a lower limit of  $7 \text{ nM}$   $\text{O}_2$  has been inferred (54) and aerobic respiration in bacteria continues down to  $3 \text{ nM}$  (55). The lower limit proposed here of  $> 0.4 \mu\text{M}$   $\text{O}_2$  in near-shore environments during the GOE therefore suggests that  $\text{O}_2$  levels were high enough for the existence of eukaryotic organisms in multiple basins over a long period. However, these limits are very close to the metazoan  $\text{O}_2$  threshold and so it is quite possible (and perhaps likely) that the evolution of motile, multicellular eukaryotes was hindered by redox instability at this time (20, 56). Nonetheless, the existing data allow the possibility that the early phases of unicellular eukaryotic evolution could have been underway in the early Paleoproterozoic. Subsequently lowered oxygen levels may have delayed the eukaryotic rise to ecological abundance for more than a billion years. Without a more complete fossil record it is all but impossible to test whether this was indeed the case. Nevertheless, during the GOE the redox restriction on microbial aerobic metabolism could have been lifted over wide areas of the continental shelves for the first time in Earth's history.

## Conclusions

An increase in the abundance of Se in organic-rich shales deposited during the GOE is consistent with enhanced oxidative continental weathering at this time, and corroborates evidence from other redox-sensitive proxies (S, Mo, and U). A shift to the most positive offshore  $\delta^{82/78}\text{Se}$  values in geologic history suggests that extensive partial reduction of Se oxyanions in shallow, suboxic seawater drove the isotopic composition of residual oceanic Se heavier. Shallow-marine sediments thus acted as a sink for isotopically light Se, perhaps recorded by the negative  $\delta^{82/78}\text{Se}$  ratios found in the Weve Slate. This state of enhanced oxidative continental weathering and extensive shallow-ocean suboxia appears to have prevailed until near the end of the GOE, when plummeting Se/TOC ratios and  $\delta^{82/78}\text{Se}$  values suggest that the marine Se reservoir rapidly diminished and suboxic water masses contracted at the expense of anoxic and, possibly, strongly euxinic waters. Thus, the period from  $\sim 2.32$ – $2.1$  Ga was the first interval in Earth's history when conditions that were at least suboxic persisted on continental margins on geological timescales, perhaps supporting the early evolution of aerobically respiring life forms. The contraction of oxic and suboxic environments after the GOE may have limited the available habitats for the evolutionary radiation of eukaryotic life until the second rise of oxygen in the late Neoproterozoic.

## Methods

Samples were prepared and analyzed following the methods of Stüeken et al. (57). Rock powders were dissolved using HF,  $\text{HNO}_3$ , and  $\text{HClO}_4$ , and Se was isolated using thiol-cotton fiber columns. All analyses were conducted on a hydride-generator multicollector inductively coupled plasma mass spectrometer (Nu Instruments). Measurements were normalized using standard-sample bracketing. We note that both  $\delta^{82/76}\text{Se}$  and  $\delta^{82/78}\text{Se}$  notations are used in the literature; our data are expressed as  $\delta^{82/78}\text{Se}$  relative to National Institute of Standards and Technology reference SRM 3149 because, using our isotopic measurement method, mass 78 is much less affected by isobaric interferences than mass 76 (57). Average precision ( $1\sigma$ ) for samples was  $0.067\%$  for  $\delta^{82/78}\text{Se}$  values and  $0.022 \text{ ppm}$  for Se concentrations.  $\delta^{82/78}\text{Se}$  values for international reference material SGR-1 and in-house standard

UW-McRae were  $+0.12 \pm 0.18\%$  ( $1\sigma$ ,  $n = 5$ ) and  $+0.85 \pm 0.18\%$  ( $1\sigma$ ,  $n = 27$ ), respectively, which agree well with published values (22, 23).

TOC analysis followed Stüeken (58). Carbonate was removed from rock powders via acidification with HCl. Decarbonated powders were analyzed on a Costech ECS 4010 Elemental Analyzer coupled to a continuous flow isotope-ratio mass spectrometer (Finnigan MAT253) via a ThermoFinnigan ConFlo III. Average precision for TOC measurements was 0.17% ( $1\sigma$ ,  $n = 49$ ).

**ACKNOWLEDGMENTS.** We thank Aivo Lepland, Chris Reinhard, Pavel Medvedev, Luke Ootes, Frantz Ossa-Ossa, New Millennium Iron, Cliffs Natural Resources, and

the Geological Survey of Botswana for access to samples critical to this work. We thank the University of Washington Isotope Geochemistry Lab for technical support. Funding for this work was provided by National Science Foundation (NSF) Grant EAR-0921580, NSF Frontiers in Earth System Dynamics Grant 1338810, and NASA Grant NNX16AI37G to R.B., as well as NSF Grant EAR-05-45484, NASA Astrobiology Institute Award NNA04CC09A, and a Natural Sciences and Engineering Research Council of Canada Discovery and Accelerator Grant (to A.B.). M.A.K. acknowledges support from an NSF Graduate Research Fellowship. E.E.S. is supported by a NASA Postdoctoral Fellowship. Additional support was provided by the NASA Astrobiology Institute Virtual Planetary Laboratory team Grant NNA13AA93A.

- Holland HD (1984) *The Chemical Evolution of the Atmosphere and Oceans* (Princeton Univ Press, Princeton).
- Lyons TW, Reinhard CT, Planavsky NJ (2014) The rise of oxygen in Earth's early ocean and atmosphere. *Nature* 506(7488):307–315.
- Bekker A, Holland HD (2012) Oxygen overshoot and recovery during the early Paleoproterozoic. *Earth Planet Sci Lett* 317:295–304.
- Schidlowski M, Trurnit P (1966) Drucklösungserscheinungen an Geröllpyriten aus den Witwatersrand-Konglomeraten. Ein Beitrag zur Frage des diagenetischen Verhaltens von Sulfiden. *Schweiz Mineral Petrogr Mitt* 46:332–342.
- Rasmussen B, Buick R (1999) Redox state of the Archean atmosphere: Evidence from detrital heavy minerals in ca. 3250–2750 Ma sandstones from the Pilbara Craton, Australia. *Geology* 27(2):115–118.
- Cloud PE, Jr (1968) Atmospheric and hydrospheric evolution on the primitive earth. Both secular accretion and biological and geochemical processes have affected earth's volatile envelope. *Science* 160(3829):729–736.
- Farquhar J, Bao H, Thiemens M (2000) Atmospheric influence of Earth's earliest sulfur cycle. *Science* 289(5480):756–759.
- Pavlov AA, Kasting JF (2002) Mass-independent fractionation of sulfur isotopes in Archean sediments: Strong evidence for an anoxic Archean atmosphere. *Astrobiology* 2(1):27–41.
- Bekker A, et al. (2004) Dating the rise of atmospheric oxygen. *Nature* 427(6970):117–120.
- Luo G, et al. (2016) Rapid oxygenation of Earth's atmosphere 2.33 billion years ago. *Sci Adv* 2(5):e1600134.
- Kump LR, et al. (2011) Isotopic evidence for massive oxidation of organic matter following the great oxidation event. *Science* 334(6063):1694–1696.
- Bekker A (2015) Lomagundi carbon isotope excursion. *Encyclopedia of Astrobiology*, eds Gargaud M, et al. (Springer, Berlin), 2nd Ed, p 1–5.
- Karhu JA, Holland HD (1996) Carbon isotopes and the rise of atmospheric oxygen. *Geology* 24(10):867–870.
- Schröder S, Bekker A, Beukes NJ, Strauss H, Van Niekerk HS (2008) Rise in seawater sulphate concentration associated with the Paleoproterozoic positive carbon isotope excursion: Evidence from sulphate evaporites in the 2.2–2.1 Gyr shallow-marine Lucknow Formation, South Africa. *Terra Nova* 20(2):108–117.
- Planavsky NJ, Bekker A, Hofmann A, Owens JD, Lyons TW (2012) Sulfur record of rising and falling marine oxygen and sulfate levels during the Lomagundi event. *Proc Natl Acad Sci USA* 109(45):18300–18305.
- Scott C, et al. (2014) Pyrite multiple-sulfur isotope evidence for rapid expansion and contraction of the early Paleoproterozoic seawater sulfate reservoir. *Earth Planet Sci Lett* 389:95–104.
- Hardisty DS, et al. (2014) An iodine record of Paleoproterozoic surface ocean oxygenation. *Geology* 42(7):619–622.
- Scott C, et al. (2008) Tracing the stepwise oxygenation of the Proterozoic ocean. *Nature* 452(7186):456–459.
- Partin CA, et al. (2013) Large-scale fluctuations in Precambrian atmospheric and oceanic oxygen levels from the record of U in shales. *Earth Planet Sci Lett* 369:284–293.
- Reinhard CT, Planavsky NJ, Olson SL, Lyons TW, Erwin DH (2016) Earth's oxygen cycle and the evolution of animal life. *Proc Natl Acad Sci USA* 113(32):8933–8938.
- Canfield DE, et al. (2013) Oxygen dynamics in the aftermath of the Great Oxidation of Earth's atmosphere. *Proc Natl Acad Sci USA* 110(42):16736–16741.
- Mitchell K, et al. (2012) Selenium as paleo-oceanographic proxy: A first assessment. *Geochim Cosmochim Acta* 89:302–317.
- Stüeken EE, et al. (2015) The evolution of the global selenium cycle: Secular trends in Se isotopes and abundances. *Geochim Cosmochim Acta* 162:109–125.
- von Strandmann PAP, et al. (2015) Selenium isotope evidence for progressive oxidation of the Neoproterozoic biosphere. *Nat Commun* 6:10157.
- Cutter GA (1982) Selenium in reducing waters. *Science* 217(4562):829–831.
- Stüeken EE (2017) Selenium isotopes as a biogeochemical proxy. *Rev Mineral Geochem* 82:657–682.
- Stüeken EE, Catling DC, Buick R (2012) Contributions to late Archean sulphur cycling by life on land. *Nat Geosci* 5(10):722–725.
- Johnson TM (2004) A review of mass-dependent fractionation of selenium isotopes and implications for other heavy stable isotopes. *Chem Geol* 204(3):201–214.
- Zhu J-M, Johnson TM, Clark SK, Zhu X-K, Wang X-L (2014) Selenium redox cycling during weathering of Se-rich shales: A selenium isotope study. *Geochim Cosmochim Acta* 126:228–249.
- Schilling K, Johnson TM, Wilcke W (2011) Selenium partitioning and stable isotope ratios in urban topsoils. *Soil Sci Soc Am J* 75(4):1354–1364.
- Clark SK, Johnson TM (2010) Selenium stable isotope investigation into selenium biogeochemical cycling in a lacustrine environment: Sweitzer Lake, Colorado. *J Environ Qual* 39(6):2200–2210.
- Rouxel O, Ludden J, Carignan J, Marin L, Fouquet Y (2002) Natural variations of Se isotopic composition determined by hydride generation multiple collector inductively coupled plasma mass spectrometry. *Geochim Cosmochim Acta* 66(18):3191–3199.
- Johnson TM, Bullen TD (2004) Mass-dependent fractionation of selenium and chromium isotopes in low-temperature environments. *Rev Mineral Geochem* 55(1):289–317.
- Mitchell K, Mansoor SZ, Mason PRD, Johnson TM, Van Cappellen P (2016) Geological evolution of the marine selenium cycle: Insights from the bulk shale  $\delta^{82}Se$  record and isotope mass balance modeling. *Earth Planet Sci Lett* 441:178–187.
- Wen H, et al. (2014) Selenium isotopes trace anoxic and ferruginous seawater conditions in the Early Cambrian. *Chem Geol* 390:164–172.
- Stüeken EE, Buick R, Anbar AD (2015) Selenium isotopes support free O<sub>2</sub> in the latest Archean. *Geology* 43(3):259–262.
- Anbar AD, et al. (2007) A whiff of oxygen before the great oxidation event? *Science* 317(5846):1903–1906.
- Garvin J, Buick R, Anbar AD, Arnold GL, Kaufman AJ (2009) Isotopic evidence for an aerobic nitrogen cycle in the latest Archean. *Science* 323(5917):1045–1048.
- Paulmier A, Ruiz-Pino D (2009) Oxygen minimum zones (OMZs) in the modern ocean. *Prog Oceanogr* 80(3):113–128.
- Bekker A, et al. (2008) Fractionation between inorganic and organic carbon during the Lomagundi (2.22–2.1 Ga) carbon isotope excursion. *Earth Planet Sci Lett* 271(1):278–291.
- Bekker A, Karhu JA, Kaufman AJ (2006) Carbon isotope record for the onset of the Lomagundi carbon isotope excursion in the Great Lakes area, North America. *Precambrian Res* 148(1):145–180.
- Rue EL, Smith GJ, Cutter GA, Bruland KW (1997) The response of trace element redox couples to suboxic conditions in the water column. *Deep Sea Res Part I* 44(1):113–134.
- Planavsky NJ, et al. (2014) Earth history. Low mid-Proterozoic atmospheric oxygen levels and the delayed rise of animals. *Science* 346(6209):635–638.
- Zhang S, et al. (2016) Sufficient oxygen for animal respiration 1,400 million years ago. *Proc Natl Acad Sci USA* 113(7):1731–1736.
- Knoll AH (2011) The multiple origins of complex multicellularity. *Annu Rev Earth Planet Sci* 39:217–239.
- Narbonne GM (2005) The ediacarabiota: Neoproterozoic origin of animals and their ecosystems. *Annu Rev Earth Planet Sci* 33:421–442.
- Walter MR, Oehler JH, Oehler DZ (1976) Megascopic algae 1300 million years old from the Belt Supergroup, Montana: A reinterpretation of Walcott's Helminthoidichnites. *J Paleontol* 50(5):872–881.
- Sharma M, Shukla Y (2009) Taxonomy and affinity of Early Mesoproterozoic megascopic helically coiled and related fossils from the Rohtas Formation, the Vindhyan Supergroup, India. *Precambrian Res* 173(1):105–122.
- Zhu S, et al. (2016) Decimetre-scale multicellular eukaryotes from the 1.56-billion-year-old Gaoyuzhuang Formation in North China. *Nat Commun* 7:11500.
- El Albani A, et al. (2010) Large colonial organisms with coordinated growth in oxygenated environments 2.1 Gyr ago. *Nature* 466(7302):100–104.
- Levin L, et al. (2002) Benthic processes on the Peru margin: A transect across the oxygen minimum zone during the 1997–98 El Niño. *Prog Oceanogr* 53(1):1–27.
- Breuer ER, et al. (2009) Sedimentary oxygen consumption and microdistribution at sites across the Arabian Sea oxygen minimum zone (Pakistan margin). *Deep Sea Res Part II Top Stud Oceanogr* 56(6):296–304.
- Sperling EA, Halverson GP, Knoll AH, Macdonald FA, Johnston DT (2013) A basin redox transect at the dawn of animal life. *Earth Planet Sci Lett* 371:143–155.
- Waldbauer JR, Newman DK, Summons RE (2011) Microaerobic steroid biosynthesis and the molecular fossil record of Archean life. *Proc Natl Acad Sci USA* 108(33):13409–13414.
- Stolper DA, Revsbech NP, Canfield DE (2010) Aerobic growth at nanomolar oxygen concentrations. *Proc Natl Acad Sci USA* 107(44):18755–18760.
- Johnston DT, et al. (2012) Late Ediacaran redox stability and metazoan evolution. *Earth Planet Sci Lett* 335:25–35.
- Stüeken EE, Foriel J, Nelson BK, Buick R, Catling DC (2013) Selenium isotope analysis of organic-rich shales: Advances in sample preparation and isobaric interference correction. *J Anal At Spectrom* 28(11):1734–1749.
- Stüeken EE (2013) A test of the nitrogen-limitation hypothesis for retarded eukaryote radiation: Nitrogen isotopes across a Mesoproterozoic basinal profile. *Geochim Cosmochim Acta* 120:121–139.

## Geologic Context

### *Menihék Formation, Upper Labrador Trough (ca. 1.85 Ga)*

The Menihék Formation of the Labrador Trough in eastern Canada is the youngest division of the Knob Lake Group and overlies the ca. 1.88 Ga Sokoman Iron Formation (1, 2). It was deposited in a deep-water setting along the eastern margin of the Superior craton. Hoffman (3) regarded this unit as foreland basin fill; however, correlative units along the southern margin of the Superior craton in the Animikie basin are considered to have been deposited in a back-arc basin (*e.g.*, ref. 4). Regardless of the exact tectonic setting, this formation was deposited in a deep-water, open-marine environment. The Menihék Formation consists of organic-rich, sulfidic, thinly laminated, fissile shales, slates and siltstones more than 300 m in thickness (5–7). The contact with the underlying granular iron formation is sharp with locally developed conglomerates. The sampled drill-core, 12-HR-1322D, is from the Howse River area. The age of ca. 1.85 Ga places deposition of the Menihék Formation >200 Myrs after the end of the Lomagundi carbon isotope excursion (8).

### *Union Island Group, Canada (ca. 2.1-2.0 Ga)*

The Union Island Group in the southwestern region of the East Arm basin in the Great Slave Lake area is now considered to be the lowermost unit of the Paleoproterozoic cover succession deposited on the margin of the Slave craton (9), in contrast to previous interpretations (10–13). The age of the group is poorly constrained, but is younger than the  $2217 \pm 4$  Ma Simpson Islands dikes that intrude the Archean basement but not the Union Island Group (11, 14, 15), and older than the unconformably overlying ca. 1.86 Ga Sosan Group (11, 13). The group has been subdivided (refs. 12, 14, 16) into the following from the base to the top: 1) a lower massive dolostone, locally underlain by quartzite and/or quartz pebble conglomerate, which rests on Archean granitic basement and a well-developed regolith; 2) organic-rich and sulfidic mudstone with decimeter-thick carbonate beds; 3) alkaline to sub-alkaline, asthenosphere-derived and crustally uncontaminated basalts with flows, flow breccia, pillows, and pillow breccia; 4) well-bedded and laminated upper dolostone with thin red mudstone beds at the top and locally developed, sub-alkaline pillow basalts; and 5) red and green laminated mudstone with soft-sediment deformation structures. Deposition was below the wave- and storm-base and possibly the photic zone for the most of the succession with the exception of the upper part of the unit 4 and unit 5. Carbonates of the first and second units have highly positive carbon isotope values, comparable to carbonates deposited during the Lomagundi carbon isotope excursion, whereas carbonates of the fourth unit have carbon isotope values close to 0‰ V-PDB. We therefore consider that the black shales analyzed in this study – collected from the second unit – were deposited in the aftermath of the Lomagundi carbon isotope excursion, after ca. 2.11-2.06 Ga (17). Samples were collected from outcrops on Union Island.

*Zaonega Formation, Karelia, Russia (ca. 2.1-2.0 Ga)*

The Zaonega Formation of Karelia, Russia comprises a 1500 m thick sequence of basaltic tuffs, siltstones, mudstones, and cherts. The Upper Zaonega sub-formation contains the majority of the organic-rich shales in the Zaonega Formation (18). It is from these horizons that samples were selected for Se analysis.

The minimum age of the Zaonega Formation is constrained by dolerite sills that are thought to be co-magmatic with volcanics of the overlying Suisar Formation, and yield U-Pb ages of  $1983 \pm 6.5$  and  $1984 \pm 8$  Ma (19). In the Onega Basin, the Zaonega Formation lies disconformably above the Tulomozero Formation, which contains isotopically heavy carbonates ( $>+10\%$   $\delta^{13}\text{C}$ ) – consistent with deposition during the Lomagundi carbon isotope excursion (8). A carbonate Pb-Pb age of  $2090 \pm 70$  Ma for the Tulomozero Formation (20) suggests that the Zaonega Formation was deposited during the latest stages of the GOE/LE (ca. 2.11-2.06 Ga, ref. 17). This is further supported by smaller carbon isotope enrichments seen in carbonates of the Lower Zaonega sub-formation than in the Tulomozero Formation (up to  $+7.9\%$   $\delta^{13}\text{C}$ ; refs. 4, 5).

Samples analyzed in this study come from three drill cores: 13A, 5190 and 175. Core 13A was drilled in the Onega Basin as part of the Fennoscandia Arctic Russia-Drilling Early Earth Program (FAR-DEEP). These cores have been studied for C, N, Mo and U isotopes as well as Fe speciation (23, 24). The C isotope trends were used to identify the Shunga-Francevillian anomaly (23), and were argued to reflect a widespread decrease in environmental oxygen levels in the wake of the GOE. While post-depositional alteration rendered the Fe speciation data difficult to interpret, Mo isotopes corroborated the story of deoxygenation (24), suggesting deposition in a euxinic environment connected to a largely anoxic global ocean.

Cores 5190 and 175 have been studied for C, S and Mo isotopes, as well as Fe speciation. Multiple S isotope systematics have been interpreted as reflecting a smaller marine sulfate reservoir during deposition of the Zaonega Formation than during the Lomagundi excursion (25). Fe speciation data suggest that these units were deposited in an environment that was transiently euxinic (25).

*FC Member, Francevillian Series, Gabon (ca. 2.1 Ga)*

The unmetamorphosed Paleoproterozoic Francevillian Basin developed on the Archean Chaillu Block (Congo craton). Its tectonic setting is still debated with interpretations ranging from intracratonic basin (26) to foreland basin (27). Regardless of the tectonic setting, the basin was open to the global ocean. The Francevillian Series hosts carbonates recording the Lomagundi carbon isotope excursion and organic-rich shales with highly negative carbon isotope values linked to the Shunga-Francevillian anomaly (28, 29). The age of the Francevillian Series is best constrained by a U-Pb SHRIMP age for the welded tuff at the top of the FD member of  $2083 \pm 6$  Ma (30, 31). Black shales suggest deposition under anoxic and even euxinic conditions based on Fe speciation and Mo concentrations and isotope ratios (32–34); whereas sulfur and iron isotope values of diagenetic pyrites indicate access to large sulfate and dissolved Fe reservoirs (33, 35). The sampled interval in the drillcore LST-12 collared in the Lastoursville sub-basin belongs to the FC Member and straddles the end of the

Lomagundi carbon isotope excursion. The FC Member in this drillcore contains organic-rich and sulfidic shales, grey massive carbonates, and cherts. Deposition was likely below wave-base and the photic zone. Sediments passed through the oil and gas windows and migrated, solidified pyrobitumen is present in the drillcore.

*Hautes Chutes Formation, Lower Labrador Trough (ca. 2.1 Ga)*

The Hautes Chutes Formation is the lowermost unit of the Swampy Bay Subgroup, and immediately overlies carbonates of the Pistolet Subgroup (Uve and Alder formations) that have highly positive carbon isotope values recording the Lomagundi carbon isotope excursion (36). The age of this unit is between  $2169 \pm 2$  Ma, an age of the granophyre dike that intrudes the underlying Seward Subgroup but not the Swampy Bay Subgroup (37), and ca. 1.88 Ga, the age of the overlying Sokoman Iron Formation (1, 2). It was deposited on the passive margin along the eastern boundary of the Superior craton and consists of up to 100 m of graphitic, pyritiferous, thinly laminated slate (38). The samples were collected from the drillcore 12-LR-1036D that was collared in 2012 in the Lake Raitche area.

*Sengoma Argillite Formation, Bushveld Basin, S.E. Botswana (ca. 2.2-2.1 Ga)*

The Sengoma Argillite Formation (SAF) was deposited in an offshore, open-marine environment on the Kaapvaal craton (39). Deposition evidently occurred during the Lomagundi carbon isotope excursion (8), as evidenced by highly  $^{13}\text{C}$ -enriched carbonates occurring above and below the SAF (40, 41). While there are no direct geochronologic constraints on the timing of SAF deposition, the 2.05-2.06 Ga age of the unconformably overlying Rooiberg Group and intruding Bushveld Complex confirm the inference that deposition occurred before the termination of the LE (42, 43). Thus, a depositional age of 2.2-2.1 Ga has previously been inferred for the SAF (25, 41). Studies of organic carbon isotopes in the SAF have shown a large offset between  $\delta^{13}\text{C}_{\text{carb}}$  and  $\delta^{13}\text{C}_{\text{org}}$ , implying a redox-stratified ocean that supported vigorous secondary production below the chemocline (41). Fe speciation data suggest that the SAF was deposited under mostly euxinic conditions (25), but S isotope systematics indicate that the marine sulfate reservoir had expanded considerably (25), consistent with studies of S isotopes in carbonate-associated sulfate (44).

*Wewe Slate, Chocolay Group, Marquette Range Supergroup (ca. 2.2-2.1 Ga)*

The Wewe Slate is in the uppermost Chocolay Group, and is unconformably overlain by the  $1874 \pm 9$  Ma Menominee Group (45). The Kona Dolomite conformably underlies the Wewe Slate, and contains isotopically enriched carbonates (up to  $+9.5\%$   $\delta^{13}\text{C}$ ) associated with the Lomagundi carbon isotope excursion (8, 46). In the Marquette Range of Michigan, the Kona Dolomite lies in unconformable contact with the Menominee Group, indicating the limited geographic extent of the Wewe Slate and suggesting that it was deposited during an episode of basin-deepening (46). A maximum age is derived from detrital zircon U-Pb ages of  $2288 \pm 15$  Ma for the underlying Enchantment Lake Formation in the lowermost Chocolay Group (47). The lack of tight

chronological constraints allows for a wide range of possible ages for the Wewe Slate; however, conformable contact with the underlying Kona Dolomite and cross-basinal correlations with other sections of the Marquette Range Supergroup suggest that an age of ca. 2.2-2.1 Ga seems most likely (46). The Bear Creek Hole 35, drilled by Cliffs Natural Resources, was sampled for this study.

The Wewe Slate was predominantly deposited below fair-weather wave base, but starved ripples suggest occasional sediment delivery by strong currents resulting in erosion overwhelming sediment supply (49). Additionally, the conformably underlying stromatolitic Kona Dolomite and mature Mesnard Quartzite indicate their deposition in a tidally-influenced shallow-marine environment (48). Thus, it seems possible that the Wewe Slate was deposited in a nearer-shore environment than the other shales analyzed in this study. This interpretation is supported by the lower TOC and TSe contents of the Wewe Slate compared to the other formations studied here (Fig. S1). Deposition in a near-shore environment could have allowed the Wewe Slate to capture a different Se isotope signal than that recorded by the outer shelf environments that were sampled in the other formations studied here. Accordingly, both extremely negative and extremely positive  $\delta^{82/78}\text{Se}$  values are seen in a relatively short section of the Wewe Slate section (Fig. S1). The lack of a trend across the drill core section suggests that these different values do not reflect secular evolution of the depositional environment (see main text for further discussion).

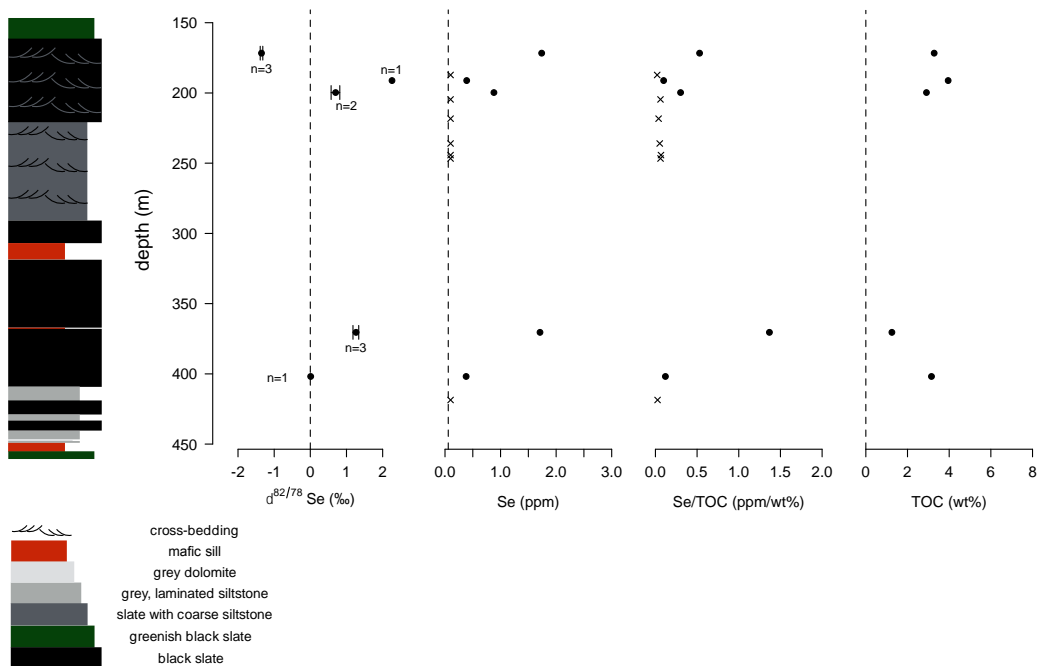


**Figure S1. Break Creek Hole 35 stratigraphic column of the Wewe Slate.** Solid symbols represent averages of multiple measurements on a single sample; crosses are samples that had insufficient Se for isotopic analysis. Error bars in Se, Se/TOC and TOC plots are omitted because they are smaller than points. No trend is seen in either  $\delta^{82/78}\text{Se}$  or TSe, suggesting that secular change in redox or depositional environment was not responsible for the spread of values. Rather, a depositional environment that straddled a chemocline with fluctuating depth could have experienced both non-quantitative and quantitative Se oxyanion reduction, causing the occurrence of very negative and very positive  $\delta^{82/78}\text{Se}$  values in <100 m of core. See text for further discussion.

## Mass-dependent fractionation of selenium isotopes

Due to the geochemical similarity of selenium and sulfur, it was once hypothesized that selenium compounds might have been subject to significant mass-independent fractionation early in Earth's history (reviewed in refs. 49, 50). Subsequent work has found no evidence for significant mass-independent fractionation of selenium isotopes (49). This dataset also displays no mass independent fractionation (Fig. S2). All deviations from the mass-dependent fractionation lines can likely be explained via residual isobaric interferences (51).

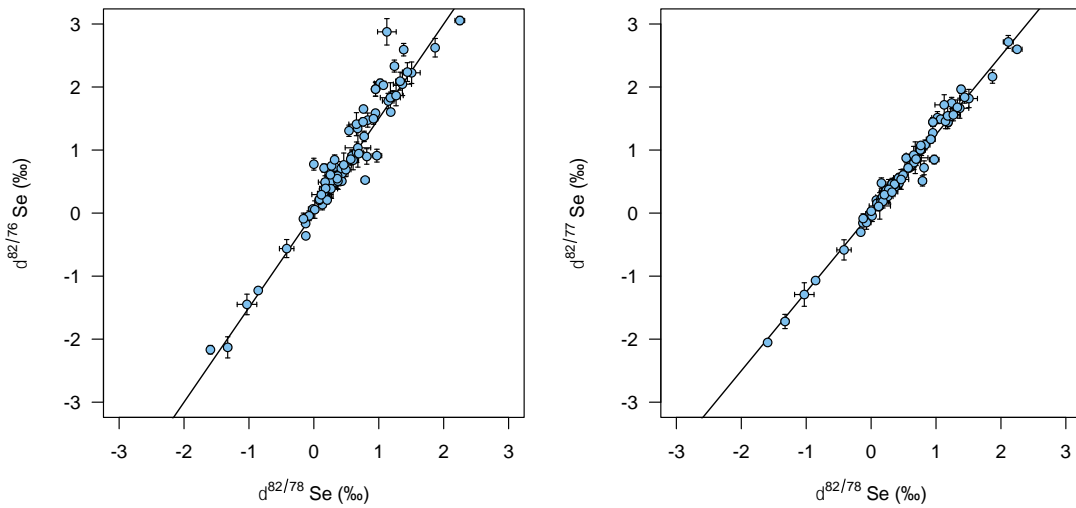


**Figure S2.** Three-isotope diagrams of  $\delta^{82/76}\text{Se}$  vs.  $\delta^{82/78}\text{Se}$  (left) and  $\delta^{82/77}\text{Se}$  vs.  $\delta^{82/78}\text{Se}$  (right). Error bars are  $1\sigma$ ; trend lines are plotted for mass-dependent fractionation (MDF). All samples display mass-dependent fractionation, with any deviations from the MDF lines likely deriving from residual interferences (see ref. 51 for discussion of method and corrections for isobaric interferences).

## References

1. Findlay JM, Parrish RR, Birkett TC, Watanabe DH (1995) U-Pb ages from the Nimish Formation and Montagnais glomeroporphyritic gabbro of the central New Québec Orogen, Canada. *Can J Earth Sci* 32(8):1208–1220.
2. Machado N, Clark T, David J, Goulet N (1997) U-Pb ages for magmatism and deformation in the New Quebec Orogen. *Can J Earth Sci* 34(5):716–723.
3. Hoffman PF (1987) Early Proterozoic Foredeeps, Foredeep Magmatism, and Superior-Type Iron-Formations of the Canadian Shield. *Proterozoic Lithospheric Evol*:85–98.
4. Schulz KJ, Cannon WF (2007) The Penokean orogeny in the Lake Superior region. *Precambrian Res* 157(1):4–25.
5. Dimroth E (1972) Stratigraphy of part of the Central Labrador Trough (between Latitude 5630' and the Height of Land), DP-154 (GM-28691). Available at: <http://www.ajsonline.org/content/272/6/487.short> [Accessed September 21, 2016].
6. Dimroth E (1970) The filling of the circum-Ungava geosyncline. *Symposium on Basins and Geosynclines of the Canadian Shield* (Geological Survey of Canada), pp 45–142.
7. Zajac IS (1974) *The stratigraphy and mineralogy of the Sokoman Formation in the Knob Lake area, Quebec and Newfoundland* (Department of Energy, Mines and Resources).
8. Bekker A (2015) Lomagundi Carbon Isotope Excursion. *Encycl Astrobiol*:1–6.
9. Sheen A, Heaman LM, Ootes L, Kjarsgaard B (2016) Union Island Group, East Arm Basin: A Record of Continental Rifting Prior to 1.9 Ga. *GAC-MAC Abstr*.
10. Hoffman PF (1968) Stratigraphy of the Great Slave Lake Supergroup (Aphebian), east arm of Great Slave Lake. *Dist Mackenzie Geol Surv Can Pap*:68–42.
11. Hoffman PF (1988) Geology and tectonics, East Arm of Great Slave Lake, Northwest Territories.
12. Hoffman PF, Bell IR, Hildebrand RS, Thorstad L (1977) Geology of the Athapuscow aulacogen, east arm of Great Slave Lake, District of Mackenzie. *Rep Act*.
13. Kjarsgaard BA, Pearson DG, DuFrane A, Heaman LM (2013) Proterozoic geology of the East Arm Basin with emphasis on Paleoproterozoic magmatic rocks, Thaidene Nene MERA study area. *Mineral and Energy Resource Assessment for the*

*Proposed Thaidene Nene National Park Reserve in the Area of the East Arm of Great Slave Lake, Northwest Territories*, eds Wright DF, Ambrose EJ, Lemkow D, Bonham-Carter GF (Geological Survey of Canada), pp 77–117.

14. Thorstad L Structure, stratigraphy, and petrology of the Union Island Group, East Arm of the Great Slave Lake, N.W.T.
15. Mumford TR, Ketchum J, Falck H, Heaman LM (2012) New geochemical, geochronological, and isotopic data for the Blatchford Lake intrusive suite and the Simpson Island dyke.
16. Goff SP The magmatic and metamorphic history of the Earth Arm, Great Slave Lake, N.W.T.
17. Karhu JA, Holland HD (1996) Carbon isotopes and the rise of atmospheric oxygen. *Geology* 24(10):867–870.
18. Medvedev PV, Philippov M, Romashkin AE, Vávra N (2001) Primary organic matter and lithofacies of siliceous shungite rocks from Karelia. *Neues Jahrb Geol Paläontol Abh* 11:641–658.
19. Filippov NB, Trofimov NN, Golubev AI, Sergeev SA, Huhma H (2007) Isotopic age data on the Koikary-Svyatnavolok and Pudozhgora sheeted intrusions. *Geol Useful Min Karelia* 10:49–68.
20. Ovchinnikova GV, et al. (2007) Pb-Pb age of Jatulian carbonate rocks: the Tulomozero Formation of southeast Karelia. *Stratigr Geol Correl* 15(4):359–372.
21. Yudovich YE, Makarikhin VV, Medvedev PV, Sukhanov NV (1991) Carbon isotope anomalies in carbonates of the Karelian Complex. *Geochem Int* 28:56–62.
22. Tikhomirova M, Makarikhin VV (1993) Possible reasons for the  $\delta^{13}\text{C}$  anomaly of lower Proterozoic sedimentary carbonates. *Terra Nova* 5(3):244–248.
23. Kump LR, et al. (2011) Isotopic Evidence for Massive Oxidation of Organic Matter Following the Great Oxidation Event. *Science* 334(6063):1694–1696.
24. Asael D, et al. (2013) Coupled molybdenum, iron and uranium stable isotopes as oceanic paleoredox proxies during the Paleoproterozoic Shunga Event. *Chem Geol* 362:193–210.
25. Scott C, et al. (2014) Pyrite multiple-sulfur isotope evidence for rapid expansion and contraction of the early Paleoproterozoic seawater sulfate reservoir. *Earth Planet Sci Lett* 389:95–104.
26. Weber F (1968) *Une série précambrienne du Gabon, le Francevillien: sédimentologie, géochimie, relations avec les gîtes minéraux associés* (Université de Strasbourg).

27. Thieblemont D, Castaing C, Billa M, Bouton P, Pr at A (2009) Notice explicative de la Carte g ologique et des Ressources min rales de la R publique gabonaise   1/1 000 000. Editions DGMG, Minist re des Mines, du P trole, des Hydrocarbures. Libreville, 384 p.
28. Gauthier-Lafaye F, Weber F (2003) Natural nuclear fission reactors: time constraints for occurrence, and their relation to uranium and manganese deposits and to the evolution of the atmosphere. *Precambrian Res* 120(1):81–100.
29. Pr at A, et al. (2011) Paleoproterozoic high  $\delta^{13}\text{C}$  dolomites from the Lastoursville and Franceville basins (SE Gabon): stratigraphic and synsedimentary subsidence implications. *Precambrian Res* 189(1):212–228.
30. Horie K, Hidaka H, Gauthier-Lafaye F (2005) U-Pb geochronology and geochemistry of zircon from the Franceville series at Bidoudouma, Gabon. *15th Annual Goldschmidt Conference*.
31. Gauthier-Lafaye F (2006) Time constraint for the occurrence of uranium deposits and natural nuclear fission reactors in the Paleoproterozoic Franceville Basin (Gabon). *Geol Soc Am Mem* 198:157–167.
32. Scott C, et al. (2008) Tracing the stepwise oxygenation of the Proterozoic ocean. *Nature* 452(7186):456–U5.
33. Albani AE, et al. (2010) Large colonial organisms with coordinated growth in oxygenated environments 2.1 Gyr ago. *Nature* 466(7302):100–104.
34. Canfield DE, et al. (2013) Oxygen dynamics in the aftermath of the Great Oxidation of Earth's atmosphere. *Proc Natl Acad Sci* 110(42):16736–16741.
35. Albani AE, et al. (2014) The 2.1 Ga Old Francevillian Biota: Biogenicity, Taphonomy and Biodiversity. *PLOS ONE* 9(6):e99438.
36. Melezhik V, Fallick A, Clark T (1997) Two billion year old isotopically heavy carbon: evidence from the Labrador Trough, Canada. *Can J Earth Sci* 34(3):271–285.
37. Rohon M-L, et al. (1993) Aphebian mafic-ultramafic magmatism in the Labrador Trough (New Quebec): its age and the nature of its mantle source. *Can J Earth Sci* 30(8):1582–1593.
38. Dimroth E (1978) Labrador trough area. *Geol Rep* 193.
39. Rouxel OJ, Bekker A, Edwards KJ (2005) Iron isotope constraints on the Archean and Paleoproterozoic ocean redox state. *Science* 307(5712):1088–1091.

40. Schidlowski M, Eichmann R, Junge CE (1976) Carbon isotope geochemistry of the Precambrian Lomagundi carbonate province, Rhodesia. *Geochim Cosmochim Acta* 40(4):449–455.
41. Bekker A, et al. (2008) Fractionation between inorganic and organic carbon during the Lomagundi (2.22–2.1 Ga) carbon isotope excursion. *Earth Planet Sci Lett* 271(1):278–291.
42. Walraven F (1997) *Geochronology of the Rooiberg Group, Transvaal Supergroup, South Africa* (Economic Geology Research Unit, University of the Witwatersrand).
43. Olsson JR, Söderlund U, Klausen MB, Ernst RE (2010) U-Pb baddeleyite ages of major Archean dyke swarms and the Bushveld Complex, Kaapvaal Craton (South Africa): correlations to volcanic rift forming events. *Precambrian Res* 183:490–500.
44. Planavsky NJ, Bekker A, Hofmann A, Owens JD, Lyons TW (2012) Sulfur record of rising and falling marine oxygen and sulfate levels during the Lomagundi event. *Proc Natl Acad Sci* 109(45):18300–18305.
45. Fralick P, Davis DW, Kissin SA (2002) The age of the Gunflint Formation, Ontario, Canada: single zircon U Pb age determinations from reworked volcanic ash. *Can J Earth Sci* 39(7):1085–1091.
46. Bekker A, Karhu JA, Kaufman AJ (2006) Carbon isotope record for the onset of the Lomagundi carbon isotope excursion in the Great Lakes area, North America. *Precambrian Res* 148(1):145–180.
47. Vallini DA, Cannon WF, Schulz KJ (2006) Age constraints for Paleoproterozoic glaciation in the Lake Superior Region: detrital zircon and hydrothermal xenotime ages for the Chocolay Group, Marquette Range Supergroup. *Can J Earth Sci* 43(5):571–591.
48. Larue DK (1981) The Chocolay Group, Lake Superior region, USA: sedimentologic evidence for deposition in basinal and platform settings on an early Proterozoic craton. *Geol Soc Am Bull* 92(7):417–435.
49. Stüeken EE, et al. (2015) The evolution of the global selenium cycle: Secular trends in Se isotopes and abundances. *Geochim Cosmochim Acta* 162:109–125.
50. Stüeken EE (2017) Selenium isotopes as a biogeochemical proxy. *Rev Mineral Geochem* 82.
51. Stüeken EE, Foriel J, Nelson BK, Buick R, Catling DC (2013) Selenium isotope analysis of organic-rich shales: advances in sample preparation and isobaric interference correction. *J Anal At Spectrom* 28(11):1734–1749.